A 6DoF hydrodynamic model for real time implementation in hybrid testing

L. Delbene, I. Bayati*, A. Facchinetti, A. Fontanella & M. Belloli

Dipartimento di Meccanica, Politecnico di Milano
Via La Masa 1, 20156, Milano, Italy.
**ilmasandrea.bayati@polimi.it*

Abstract

This work deals with the numerical approach and technical implementation of the 6-DoF hydrodynamic model, which is combined with the Politecnico di Milano HexaFloat robot (Fig.1,2), adopted for wind tunnel Hybrid/HIL tests floating offshore wind turbines.

The wind tunnel hybrid testing methodology, along with its ocean-basin counterpart [1], is currently being considered as a valuable upgrade in the model scale experiments, for its capability to reduce the effect of the typical scaling issues of such systems.

The work reports an overview of the setup and the testing methodology, presenting briefly the main challenges about the deployment on the real-time hardware and summarizing the key solving choices. A set of results related to code-to-code comparison between the optimized HIL numerical model and the reference FAST [2] computations are included, confirming the correctness of the approach.

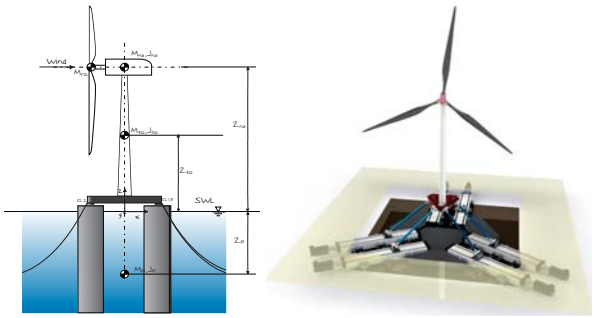

Figure 1: SWE Triple Spar concept (left) [3], whose FAST model is taken as reference, and Politecnico di Milano 6-DoF Hybrid/HIL wind tunnel setup (right), [5].

Figure 2: Hexafloat robot [5] (left) and fully controlled 1/75 aero-elastic scale model of the 10 MW DTU reference wind turbine (right), [6], [7].

1 Numerical model

Equations of motions:

$$[M_s + A_\infty]\,\ddot{\underline{x}} + [R_s]\,\dot{\underline{x}} + [K_s]\,\underline{x} = \underline{F}_{hydro} + \underline{F}_{aero} \tag{1}$$

aerodynamic forces $\underline{F}_{aero}$ measured by dynamometric balance $\underline{F}_{bal}$ placed at the tower's base combined with a correction $\underline{F}_{corr}$ due to inertial and gravitational contributions of the scale model (no Froude scaling):

$$\underline{F}_{aero} = \underline{F}_{bal} + \underline{F}_{corr} \tag{2}$$

$$\underline{F}_{corr} = [M_t]\ddot{\underline{x}} + [K_t]\underline{x} \tag{3}$$

$$\underline{F}_{hydro} = \underline{F}_{rad} + \underline{F}_{diff} + \underline{F}_{visc} + \underline{F}_{moor} \tag{4}$$

Platform radiation, diffraction and viscous forces ($\underline{F}_{rad}$, $\underline{F}_{diff}$ and $\underline{F}_{visc}$) are implemented as in [4] (extended to 6 DoF). Mooring line forces $\underline{F}_{moor}$ are included through a lumped-mass model, as in [8], where the internal nodes' contributions are: tensile load $\underline{T}$, damping $\underline{C}$, weight $\underline{W}$, contact with seabed $\underline{B}$ and viscous drag forces $\underline{D}$, depending on the nodes' position $\underline{r}$ and/or velocities $\dot{\underline{r}}$.

$$[M(\underline{r})]\,\ddot{\underline{r}} = \underline{F}_{moor}(\underline{r},\dot{\underline{r}}) = \underline{T}_{i+1/2}(\underline{r}) - \underline{T}_{i-1/2}(\underline{r}) + \underline{C}_{i+1/2}(\dot{\underline{r}},\underline{r}) - \underline{C}_{i-1/2}(\dot{\underline{r}},\underline{r}) + \underline{W}_i + \underline{B}_i(\dot{\underline{r}},\underline{r}) + \underline{D}_{p_i}(\dot{\underline{r}}) + \underline{D}_{q_i} \tag{5}$$

The mass matrix $[M]$ includes also the hydrodynamic added masses of each node $[a_i]$:

$$[M(\underline{r})] = [m] + [a(\underline{r})] \tag{6}$$

2 Modelling optimization

Simplification of the model, without loosing physical consistency, is required due to real-time constraints. As an example, the importance of each contribution of Eq.5 is evaluated for combined decay tests.

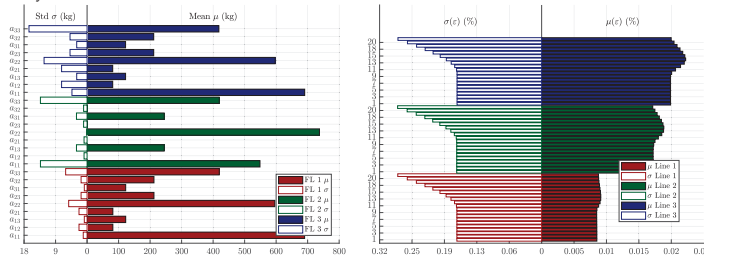

Figure 3: Added mass $[a_i]$ contribution (Eq.6) for the node # 20 for the combined decay tests $\underline{x} = \{x, y, z, \varphi, \vartheta, \psi\}^T = \{20\,m, 20\,m, 10\,m, 15°, 15°, 15°\}^T$ (left) and strain ϵ contribution for the internal nodes (#2-20) in the same decay tests (right).

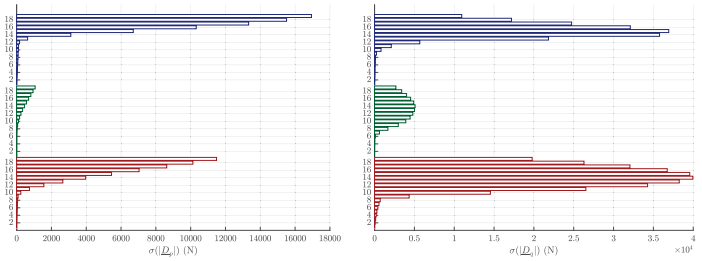

Figure 4: Viscous transverse D_p (left) and tangential D_q (right) damping contribution for the internal nodes (#2-20) in the combined decay tests $\underline{x} = \{x, y, z, \varphi, \vartheta, \psi\}^T = \{20\,m, 20\,m, 10\,m, 15°, 15°, 15°\}^T$.

	1	2	3	4	5	6	7	8	9	10	11	12	13	14	15	16	17	18	19	20	21
M	△	–	–	–	–	–	–	–	–	–	–	–	–	–	–	–	–	–	–	–	△
T	△	–	–	–	–	–	–	–	–	–	–	–	–	–	–	–	–	–	–	–	△
C	△	–	–	–	–	–	–	–	–	–	–	–	–	–	–	–	–	–	–	–	△
D_p	△	✗	✗	✗	✗	✗	✗	✗	✗	✓	✓	✓	✓	✓	✓	✓	✓	✓	✓	✓	△
D_q	△	✗	✗	✗	✗	✗	✗	✗	✗	✓	✓	✓	✓	✓	✓	✓	✓	✓	✓	✓	△
B	△	–	–	–	–	✓	✓	✓	✓	✓	✓	✓	✓	✓	✗	✗	✗	✗	✗	✗	△

Table 1: Summary of the inclusion in the model of the various mooring line's force contributions from the internal nodes, from anchor (△) to fairlead (△): constant nodes (–), potentially constant (–), varying (✓) and neglected (✗). Nodes (–) are kept variable due to numerical (integration) issues.

	f (Hz) HIL	f (Hz) FAST	p HIL	p FAST	q HIL	q FAST
Surge	0.0052	0.0050	0.24	0.28	0.039	0.033
Sway	0.0049	0.0049	0.26	0.30	0.034	0.028
Heave	0.0628	0.0628	0.31	0.31	0.015	0.015
Roll	0.0360	0.0361	0.38	0.32	-0.059	-0.018
Pitch	0.0380	0.0380	0.35	0.29	-0.037	0.001
Yaw	0.0134	0.0134	0.10	0.10	0.014	0.017

Table 2: Summary of the comparison between the real-time HIL model and the reference FAST model, including the natural frequencies f, the linear and quadratic damping parameters p and q.

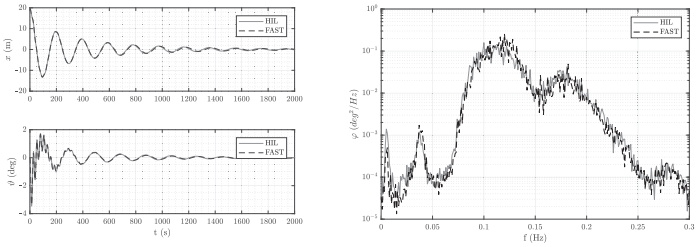

Figure 5: Surge x and pitch ϑ decay comparison (left) and pitch ϑ PSD comparison for irregular sea, $H_s = 2.2m$ and $T_p = 8s$ (right).

3 Conclusions

In Fig.5 the free decay and irregular sea results results are reported to compare the HIL model to the reference FAST one, for a subset of selected DoF, that are those envisaging the most significant amplitudes. The HIL model shows an almost overlapped behaviour. The same conclusions can be drawn looking at Tab.2, which reports the corresponding natural frequencies, linear and quadratic damping p and q, respectively defined as intercepts and slope of the graph $\frac{\Phi_n - \Phi_{n+1}}{1/2(\Phi_n + \Phi_{n+1})}$ Vs $\frac{1}{2}(\Phi_n + \Phi_{n+1})$, being Φ_n and $+\Phi_{n+1}$ the peaks of two consequent cycles of the DoF.

Tab.2 confirms the correctness of the procedure reported, where very close values between HIL and FAST can be seen. This confirms that the sensitivity analysis, supporting the definition of the simplified real-time model, can be considered satisfactory.

References

[1] Bachynski, Erin Elizabeth; Thys, Maxime; Sauder, Thomas Michel; Chabaud, Valentin Bruno; Sther, Lars Ove. (2016) *"Real-time hybrid model testing of a braceless semi-submersible wind turbine. Part II: Experimental results.* ASME 2016 35th International Conference on Ocean, Offshore and Arctic Engineering - Volume 6: Ocean Space Utilization; Ocean Renewable Energy.

[2] Jonkman J., Buhl Jr. M., *"FAST users guide"*, NREL TechRep, August 2005.

[3] Lemmer F, Amann F, Raach S et al., *"Definition of the SWE- TripleSpar Floating Platform for the DTU 10MW Reference Wind Turbine"*, Technical report, University of Stuttgart, 2016.

[4] Bayati, I., Belloli, M., Facchinetti, A. *"Wind tunnel 2-DOF hybrid/HIL tests on the OC5 floating offshore wind turbine* (2017) Proceedings of the International Conference on Offshore Mechanics and Arctic Engineering - OMAE, 10,

[5] Bayati, I., Belloli, M., Ferrari, D., Fossati, F., Giberti, H. *"Design of a 6-DoF robotic platform for wind tunnel tests of floating wind turbines* (2014) Energy Procedia, 53 (C), pp. 313-323.

[6] Bayati, I., Belloli, M., Bernini, L., Zasso, A. *"Aerodynamic design methodology for wind tunnel tests of wind turbine rotors* (2017) Journal of Wind Engineering and Industrial Aerodynamics, 167, pp. 217-227.

[7] Bayati I, Belloli M, Bernini L et al., *"Scale model technology for floating offshore wind turbines"*, IET Renewable Power Generation, 2017.

[8] Matthew Hall, Andrew Goupee, *"Validation of a lumped-mass mooring line model with DeepCwind semi submersible model test data"*, Technical report, University of Maine, 2015